Cell, Vol. 104, 619–629, February 23, 2001, Copyright ©2001 by Cell Press

TBX1 Is Responsible for Cardiovascular Defects in Velo-Cardio-Facial/DiGeorge Syndrome

Sandra Merscher,[1,12] Birgit Funke,[1,12] Jonathan A. Epstein,[4,12] Joerg Heyer,[1] Anne Puech,[2] Min Min Lu,[4] Ramnik J. Xavier,[8] Marie B. Demay,[7] Robert G. Russell,[3] Stephen Factor,[3] Kazuhito Tokooya,[5] Bruno St. Jore,[2] Melissa Lopez,[1] Raj K. Pandita,[1] Marie Lia,[1] Danaise Carrion,[1] Hui Xu,[2] Hubert Schorle,[9] James B. Kobler,[10] Peter Scambler,[6] Anthony Wynshaw-Boris,[5] Arthur I. Skoultchi,[2] Bernice E. Morrow,[1,11] and Raju Kucherlapati[1,11]

[1]Department of Molecular Genetics
[2]Department of Cell Biology
[3]Department of Pathology
Albert Einstein College of Medicine
1300 Morris Park Avenue
Bronx, New York 10461
[4]Cardiovascular Division
University of Pennsylvania
Philadelphia, Pennsylvania 19104
[5]Department of Medicine
UCSD School of Medicine
La Jolla, California 92093
[6]Institute for Child Health
University of London College of Medicine
London, United Kingdom
[7]Endocrine Unit
[8]Department of Molecular Biology
Massachusetts General Hospital
Boston, Massachusetts 02114
[9]Foschungszentrum Karlsruhe
Institut fuer Toxikologie und Genetik
Postfach 3640
76133 Karlsruhe
Germany
[10]H. P. Mosher Laryngological Research Laboratory
Department of Otology and Laryngology
Harvard Medical School
Massachusetts Eye and Ear Infirmary
243 Charles Street
Boston, Massachusetts 02114

Summary

Velo-cardio-facial syndrome (VCFS)/DiGeorge syndrome (DGS) is a human disorder characterized by a number of phenotypic features including cardiovascular defects. Most VCFS/DGS patients are hemizygous for a 1.5–3.0 Mb region of 22q11. To investigate the etiology of this disorder, we used a cre-loxP strategy to generate mice that are hemizygous for a 1.5 Mb deletion corresponding to that on 22q11. These mice exhibit significant perinatal lethality and have conotruncal and parathyroid defects. The conotruncal defects can be partially rescued by a human BAC containing the *TBX1* gene. Mice heterozygous for a null mutation in *Tbx1* develop conotruncal defects. These results together with the expression patterns of Tbx1 suggest a major role for this gene in the molecular etiology of VCFS/DGS.

Introduction

Velo-cardio-facial/DiGeorge syndrome (VCFS, MIM 192,430/DGS, MIM 188,400) is a complex developmental disorder associated with cardiac outflow tract abnormalities, mild facial dysmorphology, velopharyngeal insufficiency, submucous cleft palate, thymic, and parathyroid gland hypoplasia or aplasia (DiGeorge, 1965; Shprintzen et al., 1978; Goldberg et al., 1993). Many of the structures affected in the patients are derived from the pharyngeal arches. Ablation of cardiac neural crest cells that migrate into the pharyngeal arches results in malformations similar to those observed in VCFS/DGS patients (Kirby et al., 1983; Bockman and Kirby, 1984; Bockman et al., 1987; Kirby and Waldo, 1990). It, therefore, seems possible that VCFS/DGS may result from improper migration or function of neural crest cells resulting in anomalies of the pharyngeal arch derivatives.

Most VCFS/DGS patients are hemizygous for a 3 Mb region on human chromosome 22 (HSA22q11) while others have a smaller 1.5 Mb nested deletion (Morrow et al., 1995; Carlson et al., 1997). These observations suggested that haploinsufficiency of one or more genes on human chromosome 22 is responsible for its etiology. Several different approaches have been used to identify candidate genes in the 1.5 Mb deleted region. With the completion of the sequence of chromosome 22 (Dunham et al., 1999), as well as traditional approaches, 24 genes have been identified (Figure 1A). Despite intense efforts, the gene(s) responsible for the main clinical findings of DGS/VCFS has not yet been identified.

To extend the human molecular genetic approaches to identify the VCFS/DGS gene(s), we and others initiated efforts to generate deletions in mice in the region on mouse chromosome 16 (MMU16) that corresponds to the 1.5 Mb region of HSA22q11 (Figure 1B). Kimber et al. (1999) generated mice with a 150 kb deletion covering the proximal part of the 1.5 Mb deleted region. Mice hemizygous for this deletion were normal. Lindsay et al. (1999) described mice carrying a hemizygous deletion of an estimated 1.2 Mb region from *Es2* to *Ufd1l* on MMU16. This region contains the orthologs of 18 genes present in the human 1.5 Mb region and one nonorthologous gene, *Vpreb2.* The mutant mice, referred to as Df1/+ mice, had cardiac outflow tract defects similar to those observed in VCFS/DGS patients and some hemizygous mice died soon after birth. These results suggested that critical genes for these defects are located in this region. We recently described mice with a 550 kb deletion from *Idd* to *Arvcf* on MMU16 (Puech et al., 2000) that overlaps significantly with the region deleted in the Df1/+ mice (Figure 1B). These mice did not exhibit

[11]To whom correspondence should be addressed (email: kucherla@aecom.yu.edu or morrow@aecom.yu.edu).
[12]These three investigators contributed equally to this work.

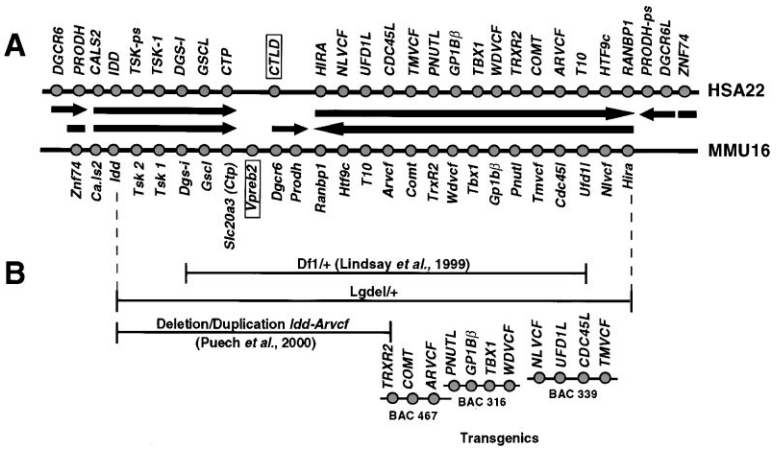

Figure 1. Map of a Part of Human Chromosome 22q11 (HSA22q11) and Its Corresponding Region on Mouse Chromosome 16 (MMU16)

(A) The relative order of genes on HSA22q11 and the orthologous genes on MMU16 are shown. Genes are indicated by circles. Arrows show differences in gene organization between the two species. Genes localized between *IDD* and *CTP* show the same order whereas genes localized between *RANBP1* and *HIRA* are inverted in mouse compared to human. *DGCR6* and *PRODH* are located proximal to *IDD* in human but inserted between *Slc20a3* and *Ranbp1* in mice. Nonorthologous genes are boxed

(B) Mouse models that have been generated are shown in the lower part of the figure.

conotruncal abnormalities, allowing us to exclude 13 genes in this region as being solely responsible, when haploinsufficient, for the outflow tract defects.

We now report the generation and characterization of mice with a hemizygous deletion from *Idd* to *Hira* (Lgdel/+ mice), a region containing 24 genes that contains five more genes than in the Df1/+ mice. We show that nearly 50% of these mice exhibit conotruncal anomalies and that the deletion also leads to parathyroid gland aplasia and significant perinatal lethality. Attempts to complement the deletion with a duplication of the *Idd-Arvcf* region and three different BAC transgenes, that together cover the 1.5 Mb region spanned by the Lgdel, allowed us to define a 200 kb region containing four genes, *Wdvcf* (*Wdr14*, Funke et al., 2001), *Tbx1* (Chapman et al., 1996; Chieffo et al., 1997), *Gp1bβ* (Yagi et al., 1994), and *Pnutl* (McKie et al., 1997), to be critical for the conotruncal phenotypes observed in the Lgdel/+ mice. We generated mice that carry a human BAC containing these four genes. Embryos heterozygous for the transgene exhibit cardiovascular abnormalities. We also examined the expression patterns of these four genes and found that one of them, *Tbx1*, is expressed in the pharyngeal arches. Based on these data, *Tbx1* can be considered a candidate for some of the phenotypes in VCFS/DGS patients. To test this feature, we generated mice with a null mutation in the *Tbx1* gene. Mice heterozygous for this mutation developed cardiovascular defects. These results provide strong evidence that haploinsufficiency of *TBX1* is responsible for the cardiovascular defects seen in VCFS/DGS patients.

Results

Targeted In Vivo Deletion of the Chromosomal Region between *Idd* and *Hira* in Mice

To generate mice with a targeted deletion of the chromosomal region from *Idd* to *Hira* (Figure 1), we bred mice that were homozygous for the *Idd* mutant allele (Puech et al., 2000) with mice heterozygous for the *Hira* mutant allele (A. W.-B. and P. S., unpublished data). Both the *Idd* and the *Hira* mutant alleles included insertions containing loxP sites in the same orientation (Figure 2A).

To obtain mice that have the two mutant alleles on the same chromosome in *cis*, we genotyped 715 offspring from *Idd* +/−; *Hira* +/− X +/+; +/+ matings. Of these, 352 (49%) were *Idd* +/− and 352 (49%) were *Hira* +/−. The remaining 11 resulted from recombination between the *Idd* and *Hira* loci and one of them carried the mutant alleles in *cis* (cis-*Idd*/*Hira*-KO). Cis-*Idd*/*Hira*-KO mice were mated with *Zp3*-Cre transgenic mice (Lewandoski et al., 1997), to introduce the Cre transgene, and mice containing all three modifications were mated with C57BL/6 (B6) mice to delete the region from *Idd* to *Hira* (Figure 2B). From 20 such matings, we recovered 105 mice, of which 66 (63%) were wild type (WT), 13 (12%) were cis-*Idd*/*Hira*-KO, and the remaining 26 (25%) carried a chromosome with a deletion. Deletion-carrying mice were identified by a series of PCR reactions (Figure 2C). Of the 26 mice that had a deletion, 14 were mosaic and the remaining 12 were the result of a germline transmission event. We designated these deletion heterozygotes Lgdel/+.

Perinatal Lethality of Lgdel/+ Mice

In the *Idd*, *Hira*/++, *Zp3-Cre*/+ X WT crosses described above, we noted that 25% of Lgdel/+ mice, 14% of the mosaic Lgdel/+ mice, and 8% of *Idd*, *Hira*/++ mice died after birth compared to less than 2% of similar deaths among WT siblings. Examination of offspring from Lgdel/+ X WT matings confirmed the perinatal lethality of Lgdel/+ mice. Genotyping of 256 mice from 48 litters revealed that 184 (72%) of them were WT and 72 (28%) were Lgdel/+. To assess the stage of lethality of Lgdel/+ mice, we examined the genotypes of embryos at 10.5, 11.5, 12.5, and 18.5 days of embryogenesis. Lgdel/+ embryos were recovered in the expected Mendelian ratio from all stages of embryogenesis examined, suggesting that a significant percentage of the Lgdel/+ mice died at or shortly after birth. We found that several newborns die during the first day of life.

Phenotypic Analysis of the Lgdel/+ Mice

Cardiovascular Defects in Lgdel/+ Embryos

Cardiac defects are observed in ~80% of VCFS/DGS patients (Shprintzen et al., 1985; Van Mierop and Kutsche, 1986; Goldberg et al., 1993; Ryan et al., 1997) and were detected in Df1/+ mice (Lindsay et al., 1999). We examined embryos from 18.5 day pregnant B6 females that were mated with Lgdel/+ males. A total of 156 embryos

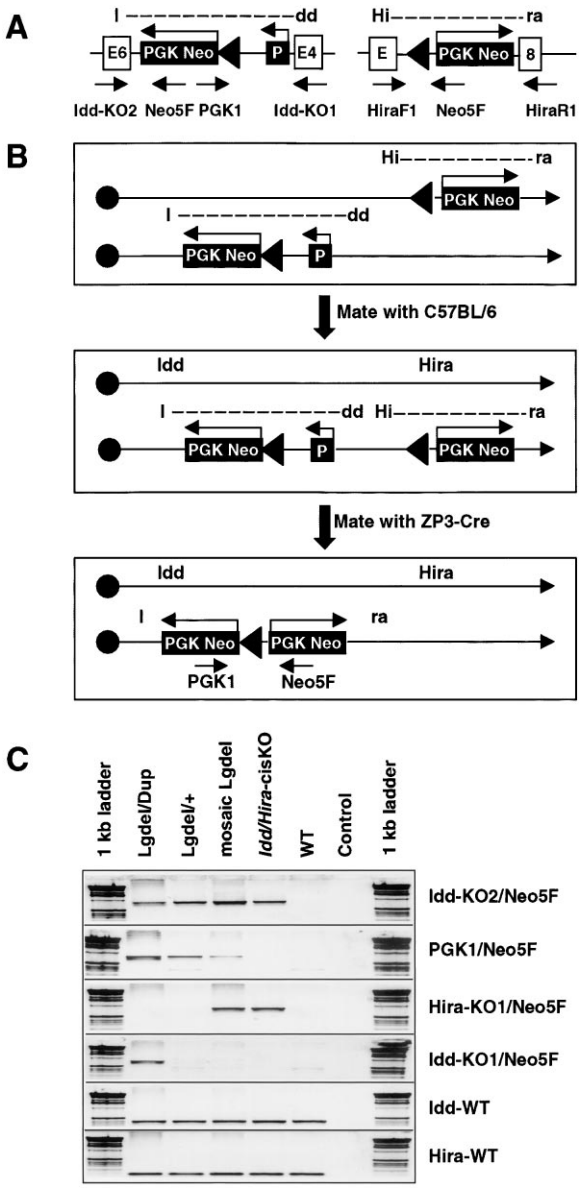

Figure 2. Strategy to Generate an In Vivo Deletion from *Idd* to *Hira*

(A) Schematic representation of the *Idd* and *Hira* targeting constructs. The exons of both genes are shown as white boxes. The PGK Neo cassettes and a solitary PGK promoter (P) are represented by black boxes and the loxP sites by black triangles. PCR primers used for genotyping and detection of the gene-targeting events are indicated by arrows.

(B) Steps involved in generating an in vivo deletion from *Idd* to *Hira*. Briefly, mice containing mutant alleles of *Idd* and *Hira* in *trans* were mated with C57BL/6 mice. The offspring are screened by PCR for a meiotic recombination event between the *Idd* and *Hira* loci and the identified cis-*Idd*/*Hira*-KO mice were mated with ZP3-Cre mice to enter the Cre transgene. To delete the region comprised within the two loxP sites (black triangles), mice containing all three modifications were then crossed with C57BL/6 mice. A deletion event can be detected by PCR using the primers for PGK1 and Neo5F as indicated by the black arrows (see also Figure 2C).

(C) Genotyping by PCR analysis. Mice containing the Lgdel chromosome, a duplication from *Idd* to *Arvcf*, or mice with a *Idd*/*Hira*-cisKO targeted chromosome can be easily distinguished from wild-type mice by PCR. The primer pairs used are indicated on the right side of the Figure (see also Experimental Procedures).

from 20 litters were analyzed. 80 embryos (51%) were hemizygous for the deletion and 76 (49%) were WT. The heart appeared normal in size and shape in all mice (data not shown). To identify vascular patterning defects, corrosion casts were prepared by injecting red and blue methylmethacrylate into the left and right ventricles, respectively. After hardening, the soft tissues were dissolved leaving a mold of the vasculature (see Experimental Procedures). Representative results are shown in Figure 3. We found that 47% of the Lgdel/+ embryos had abnormal patterning of the great vessels, while all of the wild-type littermates were normal (Figure 3A).

Twelve of the 80 Lgdel/+ embryos examined (15%) had defects that would be considered critical or lethal in human infants. These included 4 cases (5%) of a right-sided aortic arch with a left-sided ductus arteriosus (Figure 3B). In these cases, the aortic arch was posterior to the esophagus and trachea (not shown) such that a vascular ring capable of causing compression of the trachea was present. The left common carotid artery arose ectopically from the proximal ascending aorta. We observed 8 cases (10%) of complete interruption of the aortic arch, which were always of the type B variety, i.e., the interruptions occurred between the left carotid artery and the left subclavian artery (Figure 3C). In cases of complete interruption of the aortic arch, blood supply to the descending aorta is provided by flow through the patent ductus arteriosus. At birth, when the ductus closes, concomitant with increased oxygen tension, blood supply to the descending aorta would be compromised and neonatal lethality would be expected. These severe vascular defects account for at least some of the perinatal lethality observed in Lgdel/+ newborn mice.

Less severe vascular anomalies were also detected in Lgdel/+ embryos. The right subclavian artery arose ectopically in many cases. In 5 of 80 (6%) heterozygous embryos examined, the right subclavian arose from the ascending aorta instead of arising as a branch of the innominate artery (data not shown). This is considered a normal variant in humans, but we never observed this anomaly in the wild-type murine embryos examined. In 13 cases (16%), the right subclavian artery arose from the distal portion of the aortic arch and traveled posteriorly to the right foreleg indicating a retroesophageal subclavian artery (Figures 3D and 3E). In 7 cases (9%), the innominate artery was unusually long (more than twice normal) prior to the origin of the subclavian artery (Figure 3F). These defects would not be expected to cause significant morbidity or mortality.

We examined four E13.5 embryos for cardiac anomalies. We found that in one case, there was a ventricular septal defect (VSD) and associated thin myocardium. Evidence for VSD was also noted in some Lgdel/+ E18.5 embryos when methylmethacrilate was observed to quickly and easily cross the ventricular septum. VSD was reported as a feature in VCFS/DGS patients.

The cardiac and vascular defects that we observed are similar to those reported in VCFS/DGS patients and can all be related to defects in persistence or regression of aortic arches 3, 4, and 6. Neural crest cells populate these aortic arches during development, a process that is critical for regulation of the remodeling process. Similar vascular defects have been observed after ablation of neural crest in chick embryos (Kirby et al., 1983).

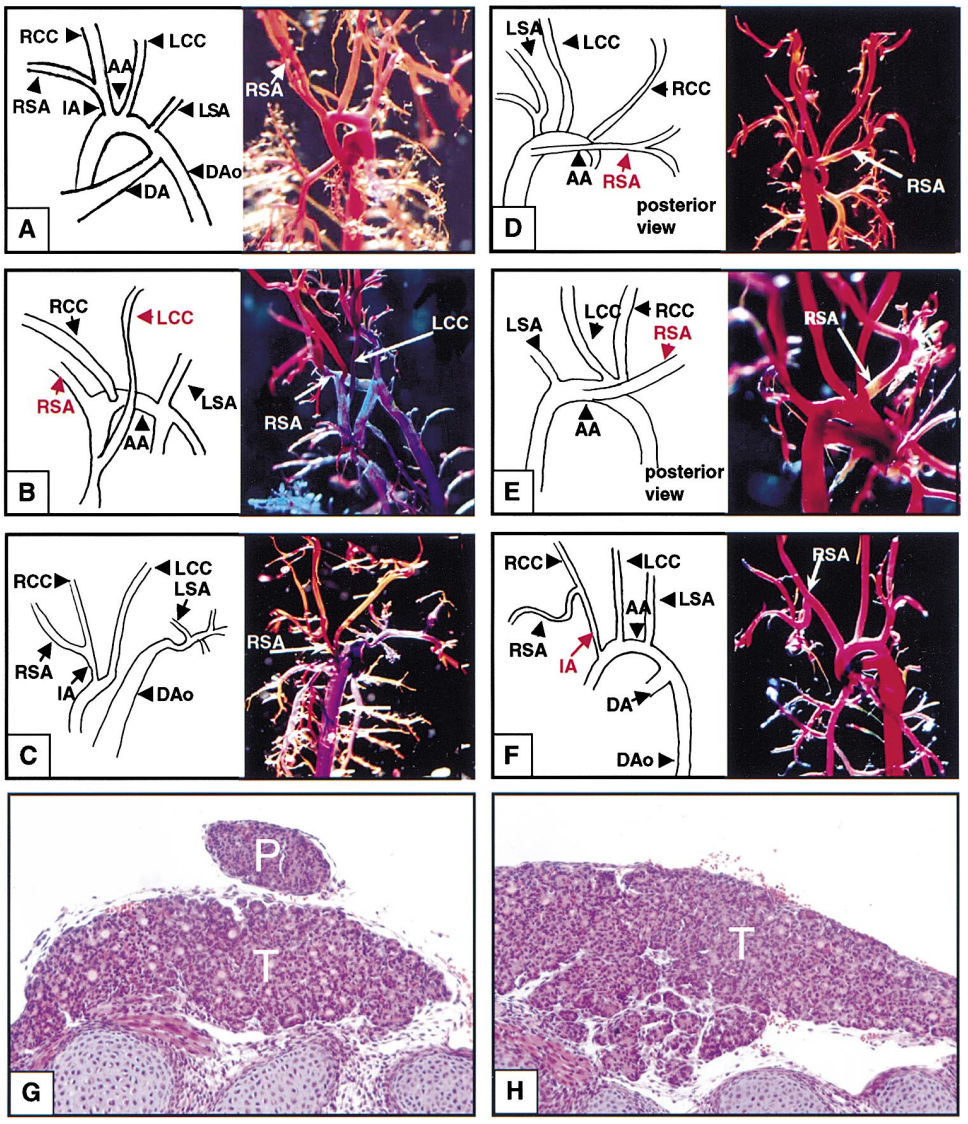

Figure 3. Cardiovascular and Parathyroid Abnormalities in Lgdel/+ E18.5 Embryos

Corrosion casts were prepared (see Experimental Procedures) from wild-type and Lgdel/+ E18.5 embryos by injection of blue acrylic into the right ventricle and red acrylic into the left ventricle.

(A) Normal anatomy in a wild-type embryo. The ascending aorta gives rise to the innominate artery (IA) that bifurcates into right subclavian artery (RSA) and right common carotid (RCC). The next arteries branching from the aortic arch (AA) are left common carotid (LCC) and left subclavian artery (LSA). (DAo = descending aorta.)

(B) Right-sided aortic arch with a left-sided ductus arteriosus.

(C) Interrupted aortic arch of the type B variety (IAA-B).

(D and E) Retro-esophageal subclavian artery. The RSA arises from the distal portion of the aortic arch and travels along a posterior route to the right arm.

(F) The innominate artery is more than twice as long as normal and arises prior to the origin of the subclavian artery.

AA = aortic arch; IA = innominate artery; RCC/LCC, right/left common carotid arteries; RSA/LSA = right/left subclavian arteries.

(G and H) Cross sections of thyroid and parathyroid from WT(G) and Lgdel/+ (H) mice stained with H&E. The absence of parathyroid was determined by examining more than 150 consecutive serial sections from each mouse.

These results suggest that haploinsufficiency of functions encoded by the region of mouse chromosome 16 between *Idd* and *Hira* regulate neural crest patterning of the aortic arches.

Phenotypic Analysis of the Thymus, Thyroid, and Parathyroid Glands in Lgdel/+ Mice

In addition to conotruncal defects, VCFS/DGS patients show absence or hypoplasia of the thymus and parathyroid glands (Goldberg et al., 1993; Ryan et al., 1997; Scuccimarri and Rodd, 1998). A deficit in thymic function can result in a deficiency of T cells and can be demonstrated by measuring the proportion of CD4+ lymphocytes. To determine whether these features are also present in the Lgdel/+ mice, we analyzed E18.5 embryos for thymic hypo- or aplasia as well as T cell immune defects. All of the 24 embryos (7 Lgdel/+ embryos and

17 WT embryos) analyzed had an intact and normal sized thymus. Flow cytometry analysis of the T cell populations in the thymus was performed using CD3, CD4, and CD8 markers and no significant differences were found in Lgdel/+ mice compared to their WT littermates (data not shown).

Rhombencephalic neural crest cells together with the endoderm of the primitive pharynx give rise to the thyroid, parathyroid, and thymus glands (Le Douarin, 1981). In histological sections, the thyroid gland is located adjacent to the rostral larynx. The parathyroid glands are embedded within the posterolateral regions of the thyroid gland. We examined a total of 13 newborns for defects in the thyroid and parathyroid glands. Out of 13 mice analyzed, 6 were WT and 7 were Lgdel/+ mice. The thyroid gland was normal in size and shape in all mice. In contrast, while the size and shape of the parathyroid glands were normal in all WT mice, 5 of 7 Lgdel/+ mice had no detectable parathyroid glands (Figures 3G and 3H).

Definition of the Critical Region for Conotruncal Defects

The *Idd-Hira* region in the mouse genome encompasses an estimated 1.5 Mb region and contains 24 genes. Our earlier studies showed that a deletion of the 550 kb *Idd-Arvcf* region did not lead to neonatal lethality in the hemizygous state nor did the mice exhibit any physical malformations including conotruncal defects at 18.5 days of embryogenesis (Puech et al., 2000). To confirm these observations and to better define the localization of the gene responsible for the phenotypes, we performed intercrosses of Lgdel/+ mice with a line that carried a duplication of the 550 kb region spanning *Idd* to *Arvcf* designated Dup (Puech et al., 2000).

We examined 141 mice from matings between Lgdel/+ mice and Dup *Idd-Arvcf* mice. Complementation of neonatal lethality observed in Lgdel/+ mice would lead to an equal proportion of mice carrying the deleted and the duplicated chromosome (Dup/Lgdel) and those that are Dup/+. Of the adult 141 mice examined, 97 (69%) were Dup/+ while 44 (31%) were Dup/Lgdel. Seven of 51 (14%) Lgdel/Dup mice died soon after birth, compared to only 1% (1/98) of their Dup/+ littermates. These results confirmed our earlier finding that the region from *Idd* to *Arvcf* is not responsible for the lethality phenotype observed in Lgdel/+ mice. These results also suggest that functional hemizygosity of the region *Arvcf-Hira*, carrying ten genes, is sufficient to lead to neonatal lethality.

BAC Transgenic Mice

To further narrow the region harboring the gene(s) responsible for conotruncal heart defects and perinatal mortality, we generated three strains of transgenic mice containing human BACs encompassing the region from *ARVCF* to *NLVCF* (Figure 1B). Human BACs were chosen to unambiguously ascertain the expression pattern of the transgenes. BAC467 contained three genes, *ARVCF*, *COMT*, and *TRXR2*. BAC316 contained four genes, *WDVCF*, *TBX1*, *GP1Bβ* , and *PNUTL*. BAC339 contained four genes, *TMVCF*, *CDC45L*, *UFD1L*, and *NLVCF*. We generated several founders from injection of each of the three BACs. Transgenics that retained the intact BAC were used for further study. Studies of expression patterns of the transgenes revealed that all of them were expressed in the same spatio-temporal pattern as their mouse counterparts (results not shown). Transgenics from BACs 467 and 339 did not have any discernable phenotypes. We observed that two lines of transgenics from BAC316, 316.23, and 316.27 had abnormal ratios of WT:Tg mice, 63:37 (n=428) and 61:39 (n=193) respectively indicating significant neonatal lethality of transgenic mice. To ascertain if this lethality is due to cardiovascular defects, we examined the cardiovascular system of E18.5 embryos by the corrosion cast technique. We examined 26 transgenic embryos and 37 WT littermates. Representative results are shown in Figure 4.

Fourteen of 26 (54%) 316.23 transgenic embryos had vascular defects involving the aortic arch and/or great vessels. Five embryos had retroesophageal subclavian arteries (Figure 4B). Three embryos had pulmonary atresia (Figure 4C). In these embryos, the pulmonary vasculature filled retrograde via the patent ductus arteriosus. In these embryos, a ventricular septal defect was present. Five embryos displayed a persistent right-sided aortic arch. In these embryos, the left carotid artery was the first major branch of the ascending aorta instead of the innominate artery (e.g., Figure 4D). A left-sided ductus arteriosus was present. Since the right-sided aortic arch travels posterior to the esophagus and trachea, a vascular ring was present with the potential for compressing these structures. In one case (Figure 4D), pulmonary atresia and a right-sided aortic arch were present in the same embryo. In this case, the ductus arteriosus anastomosed with the left subclavian artery instead of the descending aorta and served to fill the pulmonary vasculature. One newborn transgenic animal also had an interrupted aortic arch, type B (not shown). An E18.5 embryo had a complex outflow tract malformation and a ventricular septal defect (Figure 4E). All of these defects are related to inappropriate persistence or regression of aortic arch arteries three, four, and six. Migrating cardiac neural crest cells populate these three aortic arches. Therefore, the phenotypes observed are likely due to abnormalities in this aspect of development. No vascular defects were observed in any of the wild-type embryos examined. These results suggested that one or more of the genes on BAC316 are dosage sensitive and an increased level of expression of this gene(s) causes cardiovascular anomalies.

Thymus Hypoplasia and Maldescent in BAC Transgenic Mice

Incomplete migration of the thymus tissue from the pharynx into the mediastinum was detected with variable severity in BAC316.23 transgenic mice (n = 9; Figures 4F and 4G). Specifically, the two mediastinal lobes of the thymus were smaller in size and the superior borders extended as long slender strands into the neck 7–9 mm above the clavicles (n = 6; Figure 4G). Occasionally, there were small ectopic lobules at the cranial ends of these strands, which was confirmed by FACS analysis of this tissue. Fluorescence-activated cell sorting (FACS) was performed using thymocytes from the 316.23.FVB line. All thymocyte subpopulations, $CD4^+$, $CD8^+$, $CD3^+$,

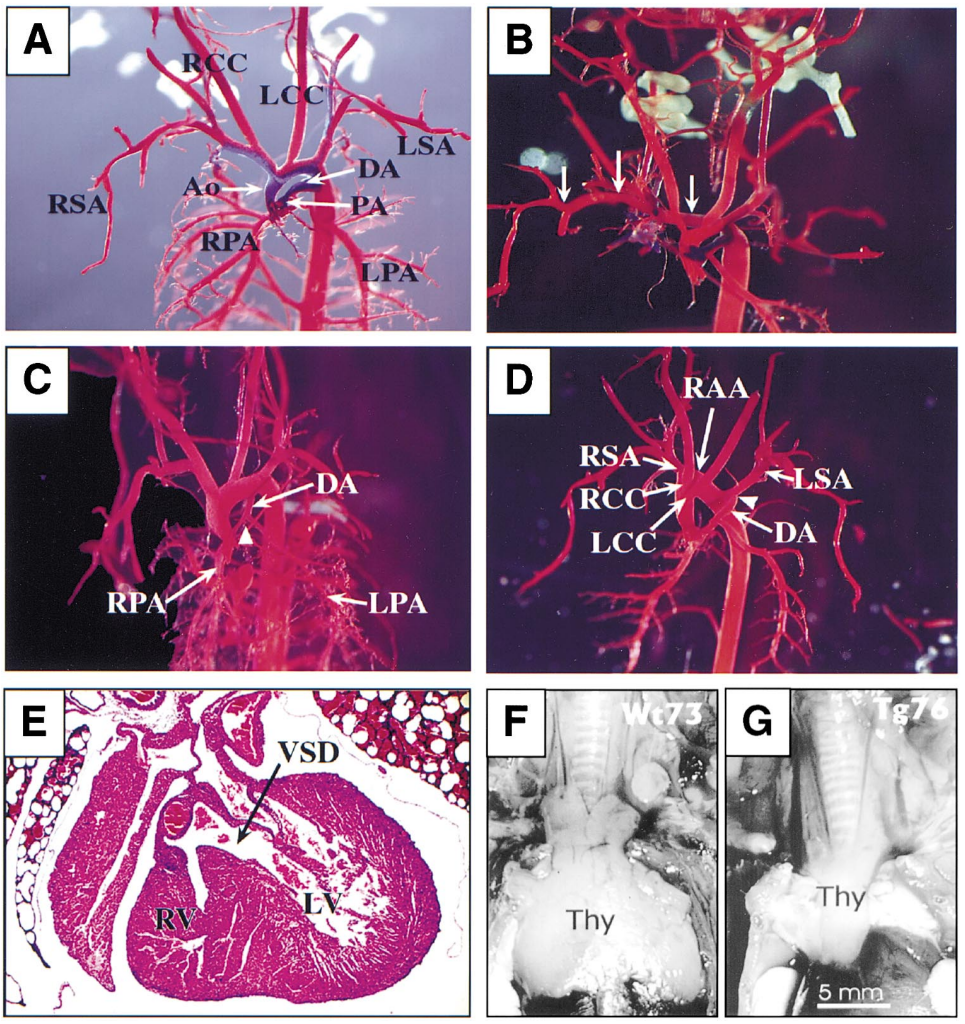

Figure 4. Cardiovascular and Thymus Defects in 316.23 Transgenic Mice

Examples of corrosion casts in E18.5 wild-type (A) and transgenic littermates (B–D). The left ventricle was injected with red methylmethacrylate and the right ventricle was injected with blue methylmethacrylate. The patent ductus arteriosus (DA) prior to birth allows mixing of red and blue. The venous system has been removed.

(A) Wild-type embryo. The ascending aorta (Ao) gives rise to the braciocephalic artery that quickly bifurcates into the right subclavian artery (RSA) and the right carotid artery (RCC). The next branch is the left carotid artery (LCC) followed by the left subclavian artery (LSA). The proximal pulmonary artery (PA) gives rise to the right and left pulmonary arteries (RPA, LPA) and the ductus arteriosus that joins the descending aorta.

(B) Transgenic embryo with a retroesophageal right subclavian artery (arrows) that originates from the descending aorta and travels posteriorly.

(C) Transgenic embryo with pulmonary atresia. The RPA and LPA fill retrograde through the DA with red methylmethacrylate. No proximal pulmonary artery is present. (Location where the proximal PA should be seen is marked with arrowhead).

(D) Transgenic embryo with a right aortic arch and pulmonary atresia. The first branch of the ascending aorta is the LCC, followed by the RCC and RSA. No brachiocephalic artery is seen. The aortic arch travels posteriorly. The RPA and LPA fill retrograde via the DA, which branches from the LSA (arrowhead) instead of from the descending aorta. This embryo represents a variant of a congenital "vascular ring" defect seen in some human infants.

(E) H&E stained cross section through the heart of an E18.5 transgenic embryo reveals a ventricular septal defect (VSD) connecting the left ventricle (LV) and right ventricle (RV).

(F and G) Representative thymi from normal (E) and transgenic littermates (F) within the body cavity of six-week-old mice.

and $CD4^{-}/CD8^{-}$, were present in normal ratios but were reduced in number in the transgenic mice compared to wild-type littermates, consistent with their smaller thymus size (data not shown). No obvious defects were found in the parathyroid glands of eight 316.23 transgenic and three wild-type littermates. Consistent with this finding, circulating parathyroid hormone levels in these transgenics were also in the normal range (60.3 +/− 11.6) showing that, in contrast to thymus development, overexpression of the transgenes did not affect parathyroid development or function.

Complementation of the Phenotypes in Lgdel/+ Mice by BAC Transgenics

To ascertain if the gene(s) on BAC316 is also responsible for the cardiovascular defects seen in VCFS/DGS pa-

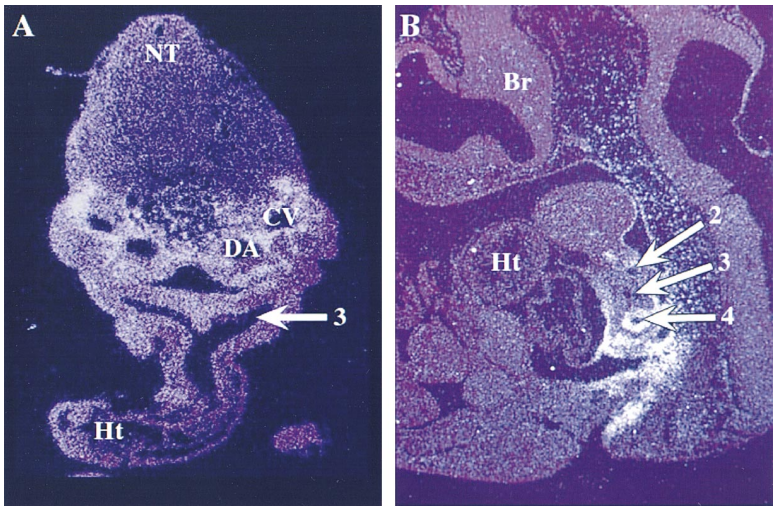

Figure 5. Expression Pattern of *Tbx1* in E10.5 Mouse Embryos

(A) Cross section of E10.5 embryo at the level of the cardiac outflow tract reveals mesenchymal expression of *Tbx1* surrounding the third aortic arch artery (3), the dorsal aorta (DA), and the cardinal vein (CV).

(B) Sagittal section of E10.5 embryo through the pharyngeal arches reveals *Tbx1* expression surrounding the aortic arch arteries (numbered 2,3,4), especially around aortic arch artery 4. Br, brain; Ht, heart; NT, neural tube. Sense probe yielded no signal (not shown).

tients, we mated the 316.23 mice with the Lgdel/+ mice. Similar crosses were also made with the two other BAC transgenics.

We analyzed 120 mice from a mating of Lgdel/+ mice and mice heterozygous for the *TMVCF-NLVCF* BAC transgenes. This mating should yield four classes of mice, two of which carry the Lgdel chromosome. Among the offspring of this mating, mice carrying the Lgdel chromosome were underrepresented (38%). Among the 45 mice carrying the Lgdel chromosome, 20 contained the transgene while the rest did not. Similar results were obtained in crosses between Lgdel/+ mice and *ARVCF-TRXR2* BAC transgenic mice. These results suggest that the genes responsible for the neonatal lethality may lie in the *Wdvcf-Pnutl* region. The 316 BAC transgenic mice, containing different numbers of transgene copies, exhibited a number of phenotypes that are similar to those observed in VCFS/DGS patients including conotruncal defects. Therefore, we examined the ability of the 1-2 copy line to complement the conotruncal defects seen in Lgdel/+ mice. From several matings of Lgdel/+ X Tg316/+ mice, we examined a total of 82 embryos. All of the +/+ and Tg316/+ embryos were normal. While 50% of the Lgdel/+ embryos had some sort of conotruncal defect, only 14% of the Lgdel/+, Tg316/+ mice had vascular anomalies. These results suggested that the transgene is capable of partially rescuing the vascular defects observed in Lgdel/+ embryos.

Expression Pattern of *Tbx1* Gene

We examined the expression patterns of the four genes on BAC316. Since VCFS/DGS is the result of developmental defects, we determined the sites of expression of the four genes by in situ hybridization of histological sections and by whole mount hybridization of E9.5–11.5 embryos. No signals were detected for *Wdvcf* and *Gp1bβ* in these embryos and *Pnutl* was expressed in the developing nervous tissue (results not shown). In contrast, *Tbx1* was expressed in the core mesenchyme of the pharyngeal arches surrounding the aortic arch arteries, the mesenchyme near the paired dorsal aortae to the pharynx and the cells surrounding the aortic arch arteries (Figure 5). Taken together, these results suggested that *TBX1* has an important role in the cardiovascular defects observed in VCFS/DGS patients.

Mice with a Mutation in *Tbx1*

To definitively assess the role of *Tbx1* in the phenotypes observed in Lgdel/+ mice, we generated mice that carry a mutation in this gene. The gene targeting construct used for this purpose is shown in Figure 6A. Correct gene targeting was verified by Southern blot analysis (Figure 6B). Embryonic stem (ES) cells carrying the modified locus were injected into B6 embryos and several chimeric mice were generated. The highly chimeric mice from two independently derived ES cell lines were mated with B6 females and 18.5 day embryos were genotyped and examined for conotruncal defects. Fourteen *Tbx1*+/− embryos and 14 wild-type littermates were examined. We observed that 7/14 (50%) of the *Tbx1*+/− embryos had abnormalities of patterning of the great vessels including two that had an abnormal origin of the right subclavian artery (RSA, Figure 7A), two with retroesophageal RSA (Figure 7B), one with an interrupted aortic arch and a retroesophageal RSA (Figure 7C), one with an RSA that arose from the pulmonary artery instead of from the systemic vasculature (Figure 7D), and one with an abnormally high aortic arch ("cervical arch", not shown). The majority of these haploinsufficient phenotypes would be compatible with postnatal survival. No vascular defects were seen in the wild-type embryos examined. These observations clearly show that reduced dosage of *Tbx1* results in conotruncal defects in mice.

Discussion

VCFS/DGS is a common developmental disorder that results from haploinsufficiency of a part of human chromosome 22. Among the most common phenotypes found in VCFS/DGS patients are cardiovascular anomalies. Since many of the organ systems affected in VCFS/DGS patients are of neural crest origin, the syndrome is considered a developmental disorder resulting from deficiency or improper migration of neural crest cells. To understand the genetic etiology and to generate a

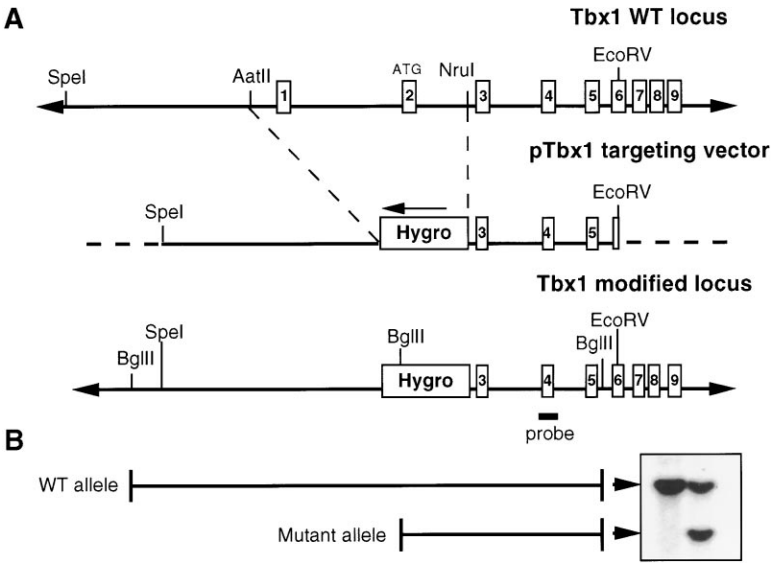

Figure 6. Strategy to Generate a Null Mutation in the Mouse *Tbx1* Gene

Hygro refers to a selection cassette containing PGK-Hygro and pNeo.

mouse model of VCFS/DGS, we generated mice carrying two deletions. One of them is designated Lgdel and encompasses a 1.5 Mb region (this report). The other deletion designated *Idd-Arvcf* deletion covers a 550 kb region (Puech et al., 2000).

We observed that the Lgdel/+ mice have three features of VCFS/DGS patients. First, there is a significant perinatal lethality among the Lgdel/+ mice. Most cases of DGS are incompatible with life (DiGeorge, 1965; Finley et al., 1977; Conley et al., 1979). Careful observation of the number of newborn pups in each mating and the number that remain after one day suggests that most, if not all, of the lethality occurs during the first day after birth. Some of the newborns were cyanotic, suggesting that death could be related to cardiovascular disorders. Similar to most human VCFS/DGS patients, a significant fraction of Lgdel/+ mice have cardiac conotruncal defects. Parathyroid abnormalities, another common feature of VCFS/DGS, were also observed in Lgdel/+ mice. Based on these results, Lgdel/+ mice can serve as a good model for at least some of the features of VCFS/DGS.

Four different deletions covering portions of mouse chromosome 16 homologous to HSA22q11 have now been described (Kimber et al., 1999; Lindsay et al., 1999; Puech et al., 2000; and this report). The largest of these is the *Idd-Hira* deletion described here and the second largest is the deletion of the *Dgs-i-Ufd1l* region (Df1) (Lindsay et al., 1999). Df1/+ mice show perinatal lethality although with a lower frequency than that observed in Lgdel/+ mice. Since five more genes are hemizygous in the Lgdel/+ mice, it is possible that the increased lethality is the result of the deletion of these additional genes. The other two smaller deletions did not cause perinatal lethality in the hemizygous state (Kimber et al., 1999; Puech et al., 2000). Taken together, these results suggest that haploinsufficiency of the region from *Arvcf-Ufd1l* is sufficient to result in perinatal lethality.

We observed that 47% of E18.5 Lgdel/+ embryos had cardiovascular defects (Figures 3B–3F). Most of the vascular anomalies seen in the Lgdel/+ embryos have also been observed in VCFS/DGS patients (Shprintzen et al., 1985; Goldberg et al., 1993; Ryan et al., 1997). We also showed that a large proportion of the Lgdel/+ mice had parathyroid abnormalities. Both cardiac and parathyroid phenotypes can be explained by an alteration in the fate of cardiac neural crest cells during embryogenesis. During gestation, pairs of branchial arch arteries form and all of the caudal arch arteries develop symmetrically until around E11.5. They then undergo dramatic remodeling to establish the embryonic asymmetric circulatory system. This remodeling process includes the asymmetrically programmed regression and persistence of specific arch arteries (for reviews see Creazzo et al., 1998; Sucov, 1998; Epstein and Buck, 2000). Aortic arch remodeling requires the presence of cardiac neural crest cells. The cardiovascular phenotypes described in the Lgdel/+ embryos can be explained by a failure of remodeling of the fourth and sixth arch arteries. Likewise, portions of the parathyroid gland are derived from the cranial neural crest. In summary, our results indicate that monosomy for the region from *Idd* to *Hira* impairs normal development of several structures derived from the neural crest, the parathyroid/heart, and great vessels emerging from the heart.

To identify the critical region harboring the gene(s) responsible for the conotruncal defects observed in the Lgdel/+ mice, we attempted to complement this deletion by breeding Lgdel/+ mice with mice carrying a duplication of the region from *Idd* to *Arvcf* and with mice containing BAC transgenes of the region from *TMVCF* to *NLVCF* (Figure 1B). We showed that neither the duplication of the region from *Idd* to *Arvcf* nor additional copies of the region from *TMVCF* to *NLVCF* or from *TRXR2* to *ARVCF* can partially rescue the phenotype observed in the Lgdel/+ mice. These results indicate that the gene(s) responsible for cardiac outflow defects and neonatal lethality is located in a region of about 200 kb containing four known genes, *WDVCF, TBX1, GP1Bβ*, and *PNUTL.* This view was substantiated by the observation that a substantial proportion of transgenic mice containing the BAC with these four genes die soon after birth and cardiac and conotruncal defects can be detected. Previously, mice with a mutation in *Gp1bβ* have been described. They were shown to mimic a human

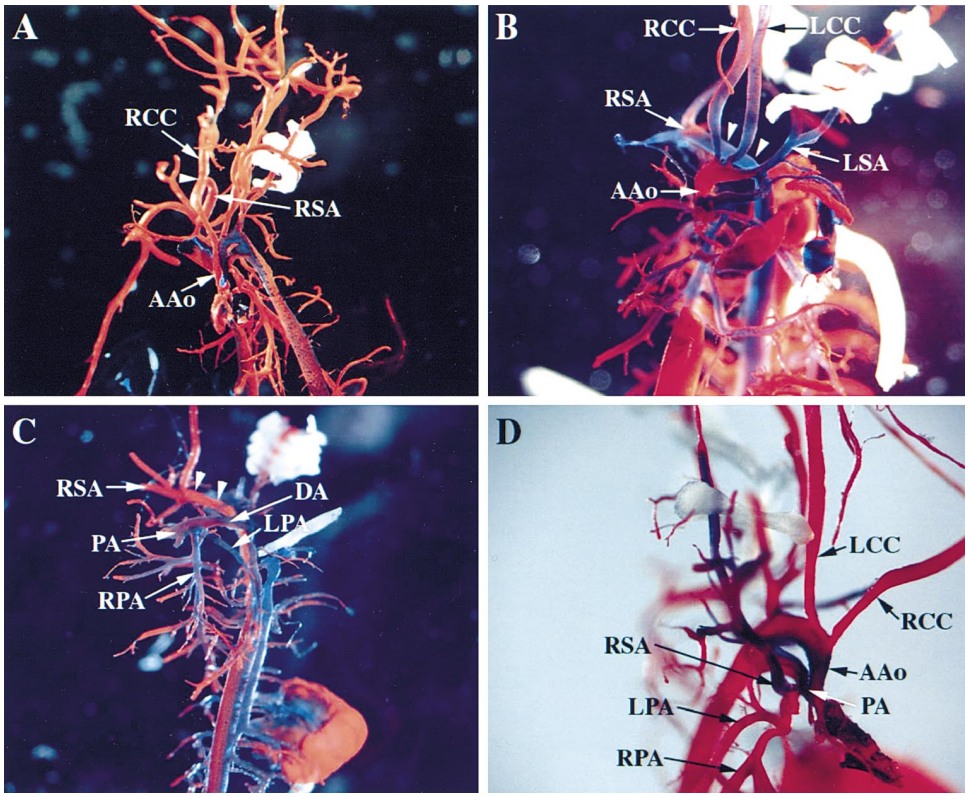

Figure 7. Conotruncal Defects in *Tbx1* +/− Mouse Embryos

(A) Abnormal origin of the right subclavian artery (RSA) is noted in this embryo (arrowhead). Note the unusually distal bifurcation of the right innominate artery into the RSA and the right common carotid artery (RCC) and the medial direction of the proximal RSA. AAo = ascending aorta.

(B) Retroesophageal RSA is evident (arrowheads). The RSA arises from the descending aorta just distal to the origin of the left subclavian artery (LSA) and travels posteriorly to the right forelimb.

(C) Complete interruption of the aortic arch with retroesophageal RSA is evident in this embryo in which the right ventricle injection only is shown. The main pulmonary artery (PA) is indicated giving rise to the right and left pulmonary arteries (RPA and LPA) and to the ductus arteriosus (DA). This injection fills the descending aorta as well as the subclavian arteries. The RSA arises from the descending aorta and travels posteriorly (arrowheads). The aortic arch is not filled by this injection. The proximal ascending aorta arising from the left ventricle gave rise to the carotid arteries (not shown). Mixing of blue and red colors in this cast indicates the presence of a ventricular septal defect.

(D) Right posterior oblique view reveals the origin of the RSA from the proximal PA at the point where the PA bifurcates into RPA and LPA. Normally, the RSA arises from the right innominate artery, which bifurcates in to RCC and RSA. LCC is left common carotid. AAo is ascending aorta.

autosomal recessive bleeding disorder Bernard-Soulier syndrome. This syndrome bears no resemblance to VCFS/DGS (Ware et al., 2000). Of the three remaining genes, *Wdvcf* is a WD40 repeat containing gene that is ubiquitously expressed at low levels in a variety of human and mouse adult and fetal tissues (Funke et al., 2001). The *Pnutl* gene also referred to as *Cdcrel-1* is expressed predominantly in the nervous system (Maldonado-Saldivia et al., 2000) and is suggested to be involved in the regulation of synaptic vesicle function (Beites et al., 1999). It is not expressed in the pharyngeal arches or outflow tract of the heart, suggesting that this gene may not be responsible for the conotruncal anomalies in the Lgdel/+ mice. *Tbx1* is a member of a phylogenetically conserved family of genes that share a common DNA binding domain, termed the T box. T box genes are transcription factors involved in the regulation of developmental processes. *Tbx1* is expressed across a wide range of embryonic stages from blastocyst through gastrulation and early organogenesis (Chapman et al., 1996). Mouse *Tbx1* is expressed during early embryogenesis in the pharyngeal arches, pouches, and otic vesicle (Chapman et al., 1996; Chieffo et al., 1997). The *Tbx* genes are a family of dosage-sensitive genes and two of its members have been associated with dominant human disorders. Mutations in *TBX5* result in Holt-Oram syndrome that is associated with heart defects (Basson et al., 1997; Li et al., 1997; Basson et al., 1999). Tbx3 mutations cause mammary-ulnar syndrome (Bamshad et al., 1997).

To test the involvement of *TBX1* in the phenotypes associated with VCFS/DGS, we generated mice with a null mutation in this gene. Mice that are hemizygous for the *Tbx1* mutation had cardiovascular phenotypes similar to those in the Lgdel/+ mice and in VCFS/DGS patients. These results clearly show that *TBX1* plays a critical developmental role in the formation of at least some of the organ systems derived from neural crest including the cardiovascular system.

It has to be noted that neither the *Tbx1* mutant heterozygotes nor the Lgdel/+ mice have all of the phenotypes observed in VCFS/DGS patients. The involvement of

other linked or unlinked genes in the manifestation of all of the phenotypes seen in VCFS/DGS patients requires additional investigation.

Experimental Procedures

Generation of *Idd* and *Hira* Heterozygous Mice

Two separate targeting vectors for the *Idd* and the *Hira* locus were constructed to generate an in vivo deletion of the chromosomal region between *Idd* and *Hira* in mice.

In one, the *Idd* locus was disrupted by homologous recombination resulting in the deletion of a 2 kb segment including *Idd* exons 4 and 5 (Puech et al., 2000; Figure 2A) and in the second, the *Hira* locus was disrupted by deleting a 1.5 kb region including the 3′ part of exon 8 (A. W.-B. and P. S., unpublished data; Figure 2A).

A PGKNeo cassette and a loxP site in the same orientation have also been included in both targeting vectors. The vectors were transfected separately into embryonic stem (ES) cells and ES cell clones bearing the mutant alleles were used to generate chimeric mice. Heterozygous offspring for both mutant alleles were generated by further crossing the chimeric founders with B6 females.

Tbx1 Gene Targeting

The genomic sequence of *Tbx1* (GenBank Accession number AC003066) was used to generate an exon/intron and restriction enzyme map. A 13 kb SpeI-EcoRV fragment from BAC 213A6 (RPCI 21; http://www.chori.org/bacpac/) containing *Tbx1* exon 1 through part of exon 6 was subcloned into pZErO-2 (Invitrogen). The plasmid was digested with AatII and NruI to release a 4.9 kb *Tbx1* genomic fragment including exons 1 and 2 (exon 2 contained the ATG). This interval was blunt-ended and replaced with a hygromycin resistance cassette. To generate the targeted embryonic stem (ES) cell clones, 30 ug of linearized targeting vector was electroporated into 2.5×10^7 WW6 ES cells and selected for hygromycin resistance. Colonies were picked after ten days and their DNA was screened by PCR using the forward primer from the hygromycin cassette, 5′-AGGTCC CTCGAAGAGGTTCA-3′ and reverse primer from exon 6, 5′-GTC CACATAGACAACATGGAA-3′. The reaction was performed using the Expand Long Template PCR System for amplification of a 3.2 kb product (Buffer 3; Roche Pharmaceuticals). Chimeric mice were generated by injecting C57Bl/6 blastocysts with 8–12 ES cells derived from clone 7D6 or 1C3. Both lines gave rise to male chimeric animals that were mated with C57Bl/6 females. Germline transmission was demonstrated by genomic Southern blot analysis to detect the rearranged *Tbx1* locus. F1 heterozygotes were used in the analysis.

Screening of the BAC Library

High-density gridded membranes containing a BAC library (RPCI 11, 170 kb average insert size, 25× fold redundant; http://www.chori.org/bacpac) were screened with ^{32}P-labeled (random primed DNA labeling Kit, Boehringer Mannheim Corp.) PCR products correspond to six different loci within the distal half of the 1.5 Mb region deleted in VCFS/DGS patients. The positive clones were isolated and DNA was prepared (Qiagen Corp.). The ends of the identified clones were sequenced using ABI377 automated sequencing machines. Each sequence was compared to those in GenBank (http://www.ncbi.nlm.nih.gov/BLAST/) to determine the exact size and location of the BACs in the genomic sequence of chromosome 22.

Purification of BAC DNA and Generation of Transgenic Mice

BAC DNA was isolated using an alkaline lysis and cesium chloride gradient ultracentrifugation protocol. Rnase-treated DNA was further purified using the Endo-free Plasmid Maxi Kit (Gibco, BRL). Transfer into injection buffer was achieved by passing the DNA over a Sepharose CL4b-column (Pharmacia) that was equilibrated with injection buffer (10 mM Tris HCl, pH 7.5; 0.1 mM EDTA; 100 mM NaCl).

Circular BAC DNA was injected into the pronucleus of fertilized FVB zygotes at a concentration of 3 ng/μl. The Transgenics and Gene Targeting Facility of the Albert Einstein College of Medicine performed all injections. Founders were identified by two methods: Primers BACT7-F (AATGCTCATCCGGAGTTCC) and BACT7-R (ACT GGTGAAACTCACCCAGG) were used to amplify the T7 end of BAC vector pBACe3.6 (http://www.chori.org/bacpac/home.htm). Primers BACSP6-F (GCTGCAGATCCCTAAACAGC) and BAC probe-R (AGC GCTATATGCGTTGATGC) were used to generate a PCR product from the SP6 end of the same vector that was also used as a probe for genomic Southern analysis (see below). FVB or C57B1/6 mice were used to establish colonies from the founder animals.

Analysis of Embryos and Mice

Mice were kept on a 12 hr light/dark cycle and noon of the plug date was considered as 0.5 d.p.c. DNA for genotyping was prepared from tail using the DNeasy Tissue Kit from Qiagen and following the instructions of the manufacturer.

Genotyping by PCR

The following primers were used for genotyping of the mice and embryos:

PGK1, GCTAAAGCGCATGCTCCAGAC; Neo5F, ACCGCTATCAG GACATAGCGT;

Idd-KO1, CTGTTGTTGACACAGCACATG; 6x32t3, AACTCTACCT GTTCCTACTG;

Idd-KO2, CACGTTGTCATTCTCAGACATG; HiraR1, GTGATGC TAGTCTCTAGCTG;

HiraF1, TCTTGCAACTCTGAGAGGTC; CreF, GGACATGTTCAGG GATCGCCAGGCG; CreR, GCATAACCAGTGAAACAGCATTGCTG.

The primers were combined as follows (Figure 2C): Idd-KO2/Neo5F or Idd-KO1/PGK1 for identification of a homologous recombination event at the *Idd* locus, Idd-KO1/6x32t3 for amplification of the *Idd* wild-type allele, HiraF1/Neo5F for identification of a homologous recombination event at the *Hira* locus, and HiraF1/HiraR1 for amplification of the *Hira* wild-type allele. To amplify the junction fragment of the *Idd* and *Hira* target vectors after a deletion event, the primers PGK1/Neo5F were used. Cre-F/Cre-R primers were used for amplification of the Cre transgene. 7 ul of DNA was used as a template in the PCR reaction. The PCR conditions were 94°C for 4 min, one cycle; 58°C for 45 s, 72°C for 45 s, and 94°C for 30 s (35 cycles); 72°C for 1 min, one cycle.

Corrosion Casts

Embryos were isolated of 18.5 days pregnant B6 females inseminated by Lgdel/+ males and the heart exposed by a thoracic incision and rib removal. Batson no. 17 acrylic (Polysciences, Inc) was injected into the right and left ventricle until the entire embryonic vasculature was filled. After hardening, the tissue was removed with Maceration Solution (Polysciences, Inc) at 50°C for 72 hr. Photographs were obtained digitally and processed with Photoshop software.

Analysis of Thyroid and Parathyroid Glands

Mice were sacrificed at E18.5. The thyroid gland (with associated parathyroids) of each animal was completely resected with associated trachea, fixed and embedded in paraffin. Paraffin blocks were completely sectioned at 4–5 μm. At most, only a few sections were lost during cutting on the microtome. Sections were stained with hematoxylin and eosin, and examined at 20× magnification for the presence of easily identified parathyroid glands anywhere within the thyroid sections. One hundred to 125 sections were examined for each animal.

Immunofluorescence Staining and Flow Cytometric Analysis

Thymocytes (1×10^6) were rinsed with flow cytometry buffer (HANKS solution containing 0.1% bovine serum albumin and 0.1% sodium azide), pelleted by centrifuge, and doubly stained with phycoerythrin(PE)-labeled anti-CD4 mAb (PharMingen, San Diego, CA) and FITC-conjugated anti-CD8 mAb (PharMingen) on ice for 20 min. Cells were then washed twice with staining flow cytometry buffer. Cells were singly stained with FITC-conjugated anti-CD3 epsilon chain mAb (PharMingen). After washing, cells were fixed with 2% paraformaldehyde in PBS. Stained cells were analyzed on Epics flow cytometer (Coulter, Miami, FL).

Acknowledgments

The work described here was inspired by Robert Shprintzen and Rosalie Goldberg. We thank J. Horner and K. Chen for microinjec-

tions, L. Edelmann and T. Van De Water for scientific discussions, and J. Sterio for technical assistance. This work is supported by grants from the NIH (HD34980 to R. K., B. E. M., and A. I. S.; HL 61475, HL 62974 to J. A. E.; AI01472 to R. J. X.), the WW Smith Chartitable Trust (J. A. E.), the American Heart Association (B. M.), the British Heart Foundation (P. J. S.), and the Deutsche Forschungsgemeinschaft (H. S.).

Received January 3, 2001; revised January 29, 2001.

References

Basson, C.T., Bachinsky, D.R., Lin, R.C., Levi, T., Elkins, J.A., Soults, J., Grayzel, D., Kroumpouzou, E., Traill, T.A., Leblanc, S.J., et al. (1997). Mutations in human TBX5 cause limb and cardiac malformation in Holt-Oram syndrome. Nat. Genet. *15*, 30–35.

Basson, C.T., Huang, T., Lin, R.C., Bachinsky, D.R., Weremowicz, S., Vaglio, A., Bruzzone, R., Quadrelli, R., Lerone, M., Romeo, G., et al. (1999). Different TBX5 interactions in heart and limb defined by Holt-Oram syndrome mutations. Proc. Natl. Acad. Sci. USA *96*, 2919–2924.

Bamshad, M., Lin, R.C., Law, D.J., Watkins, W.C., Krakowiak, P.A., Moore, M.E., Franceschini, P., Lala, R., Holmes, L.B., Gebuhr, T.C., et al. (1997). Mutations in human TBX3 alter limb, apocrine and genital development in ulnar-mammary syndrome. Nat. Genet. *16*, 311–315.

Beites, C.L., Xie, H., Bowser, R., and Trimble, W.S. (1999). The septin CDCrel-1 binds syntaxin and inhibits exocytosis. Nat. Neurosci. *2*, 434–439.

Bockman, D.E., and Kirby, M.L. (1984). Dependence of thymus development on derivatives of the neural crest. Science *223*, 498–500.

Bockman, D.E., Redmond, M.E., Waldo, K., Davis, H., and Kirby, M.L. (1987). Effect of neural crest ablation on development of the heart and arch arteries in the chick. Am. J. Anat. *180*, 332–341.

Carlson, C., Sirotkin, H., Pandita, R., Goldberg, R., McKie, J., Wadey, R., Patanjali, S.R., Weissman, S.M., Anyane, Y.K., Warburton, D., et al. (1997). Molecular definition of 22q11 deletions in 151 velo-cardio-facial syndrome patients. Am. J. Hum. Genet. *61*, 620–629.

Chapman, D.L., Garvey, N., Hancock, S., Alexiou, M., Agulnik, S.I., Gibson, B.J., Cebra, T.J., Bollag, R.J., Silver, L.M., and Papaioannou, V.E. (1996). Expression of the T-box family genes, *Tbx1*-Tbx5, during early mouse development. Dev. Dyn. *206*, 379–390.

Chieffo, C., Garvey, N., Gong, W., Roe, B., Zhang, G., Silver, L., Emanuel, B.S., and Budarf, M.L. (1997). Isolation and characterization of a gene from the DiGeorge chromosomal region homologous to the mouse *Tbx1* gene. Genomics *43*, 267–277.

Conley, M.E., Beckwith, J.B., Mancer, J.F., and Tenckhoff, L. (1979). The spectrum of the DiGeorge syndrome. J. Pediatr. *94*, 883–890.

Creazzo, T.L., Godt, R.E., Leatherbury, L., Conway, S.J., and Kirby, M.L. (1998). Role of cardiac neural crest cells in cardiovascular development. Annu. Rev. Physiol. *60*, 267–286.

DiGeorge, A. (1965). A new concept of the cellular basis of immunity. J. Pediatr. *67*, 907–908.

Dunham, I., Shimizu, N., Roe, B.A., Chissoe, S., Hunt, A.R., Collins, J.E., Bruskiewich, R., Beare, D.M., Clamp, M., Smink, L.J., et al. (1999). The DNA sequence of human chromosome 22. Nature *402*, 489–495.

Epstein, J.A., and Buck, C.A. (2000). Transcriptional regulation of cardiac development: implications for congenital heart disease and DiGeorge syndrome. Pediatr. Res. *48*, 717–724.

Finley, J.P., Collins, G.F., de Chadarevian, J.P., and Williams, R.L. (1977). DiGeorge syndrome presenting as severe congenital heart disease in the newborn. Can. Med. Assoc. J. *116*, 635–640.

Funke, B., Pandita, R.K., and Morrow, B.E. (2001). Isolation and characterization of a novel gene containing WD40 repeats from the region deleted in velo-cardio-facial/DiGeorge syndrome on chromosome 22q11. Genomics, in press.

Goldberg, R., Motzkin, B., Marion, R., Scambler, P.J., and Shprintzen, R.J. (1993). Velo-cardio-facial syndrome: a review of 120 patients. Am. J. Med. Genet. *45*, 313–319.

Kimber, W.L., Hsieh, P., Hirotsune, S., Yuva, P.L., Sutherland, H.F., Chen, A., Ruiz, L.P., Hoogstraten, M.S., Chien, K.R., Paylor, R., et al. (1999). Deletion of 150 kb in the minimal DiGeorge/velocardiofacial syndrome critical region in mouse. Hum. Mol. Genet. *8*, 2229–2237.

Kirby, M.L., and Waldo, K.L. (1990). Role of neural crest in congenital heart disease. Circulation *82*, 332–340.

Kirby, M.L., Gale, T.F., and Stewart, D.E. (1983). Neural crest cells contribute to normal aorticopulmonary septation. Science *220*, 1059–1061.

Le Douarin, N.M. (1981). The Neural Crest. (Cambridge, MA: Cambridge University Press).

Lewandoski, M., Wassarman, K.M., and Martin, G.R. (1997). Zp3-cre, a transgenic mouse line for the activation or inactivation of loxP-flanked target genes specifically in the female germ line. Curr. Biol. *7*, 148–151.

Li, Q.Y., Newbury, E.R., Terrett, J.A., Wilson, D.I., Curtis, A.R., Yi, C.H., Gebuhr, T., Bullen, P.J., Robson, S.C., Strachan, T., et al. (1997). Holt-Oram syndrome is caused by mutations in TBX5, a member of the Brachyury (T) gene family. Nat. Genet. *15*, 21–29.

Lindsay, E.A., Botta, A., Jurecic, V., Carattini, R.S., Cheah, Y.C., Rosenblatt, H.M., Bradley, A., and Baldini, A. (1999). Congenital heart disease in mice deficient for the DiGeorge syndrome region. Nature *401*, 379–383.

Maldonado-Saldivia, J., Funke, B., Pandita, R.K., Schuler, T., Morrow, B.E., and Schorle, H. (2000). Expression of cdcrel-1 (Pnutl1), a gene frequently deleted in velo-cardio-facial syndrome/DiGeorge syndrome. Mech. Dev. *96*, 121–124.

McKie, J.M., Sutherland, H.F., Harvey, E., Kim, U.J., and Scambler, P.J. (1997). A human gene similar to Drosophila melanogaster peanut maps to the DiGeorge syndrome region of 22q11. Hum. Genet. *101*, 6–12.

Morrow, B., Goldberg, R., Carlson, C., Das, G.R., Sirotkin, H., Collins, J., Dunham, I., O'Donnell, H., Scambler, P., Shprintzen, R., et al. (1995). Molecular definition of the 22q11 deletions in velo-cardio-facial syndrome. Am. J. Hum. Genet. *56*, 1391–1403.

Puech, A., Saint-Jore, B., Merscher, S., Russell, R.G., Cherif, D., Sirotkin, H., Xu, H., Factor, S., Kucherlapati, R., and Skoultchi, A.I. (2000). Normal cardiovascular development in mice deficient for 16 genes in 550 kb of the velocardiofacial/DiGeorge syndrome region. Proc. Natl. Acad. Sci. USA *97*, 10090–10095.

Ryan, A.K., Goodship, J.A., Wilson, D.I., Philip, N., Levy, A., Seidel, H., Schuffenhauer, S., Oechsler, H., Belohradsky, B., Prieur, M., et al. (1997). Spectrum of clinical features associated with interstitial chromosome 22q11 deletions: a European collaborative study. J. Med. Genet. *34*, 798–804.

Scuccimarri, R., and Rodd, C. (1998). Thyroid abnormalities as a feature of DiGeorge syndrome: a patient report and review of the literature. J. Pediatr. Endocrinol. Metab. *11*, 273–276.

Shprintzen, R.J., Goldberg, R.B., Lewin, M.L., Sidoti, E.J., Berkman, M.D., Argamaso, R.V., and Young, D. (1978). A new syndrome involving cleft palate, cardiac anomalies, typical facies, and learning disabilities: velo-cardio-facial syndrome. Cleft Palate J. *15*, 56–62.

Shprintzen, R.J., Wang, F., Goldberg, R., and Marion, R. (1985). The expanded velo-cardio-facial syndrome (VCF): additional features of the most common clefting syndrome. Am. J. Hum. Genet. *37*, A77.

Sucov, H.M. (1998). Molecular insights into cardiac development. Annu. Rev. Physiol. *60*, 287–308.

Van Mierop, L.H., and Kutsche, L.M. (1986). Cardiovascular anomalies in DiGeorge syndrome and importance of neural crest as a possible pathogenetic factor. Am. J. Cardiol. *58*, 133–137.

Ware, J., Russell, S., and Ruggeri, Z.M. (2000). Generation and rescue of a murine model of platelet dysfunction: the Bernard-Soulier syndrome. Proc. Natl. Acad. Sci. USA *97*, 2803–2808.

Yagi, M., Edelhoff, S., Disteche, C.M., and Roth, G.J. (1994). Structural characterization and chromosomal location of the gene encoding human platelet glycoprotein Ib beta. J. Biol. Chem. *269*, 17424–17427.